Measurement of the neutron total cross section of ^{169}Tm in the energy range of 1−110 keV and recommendation of optical model parameters*

Haolan Yang (杨皓岚)[1] Jieming Xue (薛洁明)[1] Jie Ren (任杰)[1†] Yonghao Chen (陈永浩)[2,3] Xichao Ruan (阮锡超)[1‡] Jincheng Wang (王金成)[1] Jie Bao (鲍杰)[1] Ruirui Fan (樊瑞睿)[2,3] Wei Jiang (蒋伟)[2,3] Qi Sun (孙琪)[1] Yingyi Liu (刘颖一)[1] Zhongxian Luo (罗忠献)[1] Hanxiong Huang (黄翰雄)[1]

[1]Key Laboratory of Nuclear Data, China Institute of Atomic Energy, Beijing 102413, China
[2]Institute of High Energy Physics, Chinese Academy of Sciences (CAS), Beijing 100049, China
[3]Spallation Neutron Source Science Center, Dongguan 523803, China

Abstract: The neutron total cross section (σ_t) of ^{169}Tm is of considerable importance in the design of nuclear reactors and applications of nuclear technology. However, the σ_t of ^{169}Tm is unavailable in the 5 keV to 2.3 MeV energy range in the Experimental Nuclear Reaction Data library and exhibits significant discrepancies among different Evaluated Nuclear Data libraries in the keV region. To clarify the discrepancies in the σ_t of ^{169}Tm in the keV energy region, we developed a new measurement strategy using the transmission method and the time-of-flight technique and employed it at the back-streaming white neutron beamline of the China Spallation Neutron Source. The experimental background was quantitatively determined using the saturated resonance absorption technique with a ^{7}Li-glass scintillator. The σ_t of ^{169}Tm in the 1−110 keV energy range was obtained, and the value showed good agreement with the evaluated data in the JENDL-5 library. The calculations of the optical model agree well with the results and the fine-tuned optical model parameters in TALYS validated against the 2.3–2.5 MeV data reported by Foster and Glasgow, with deviations below 5%. The results fill the experimental gap in the 5–110 keV range and thus provide valuable input for research on nuclear reactions and evaluations of nuclear data.

Keywords: total cross section, transmission, optical model parameters

DOI: 10.1088/1674-1137/ae31e1 **CSTR:** 32044.14.ChinesePhysicsC.50044106

I. INTRODUCTION

The neutron total cross section is the sum of partial cross sections for all neutron-induced reaction channels, which is valuable in nuclear reaction studies, nuclear reactor designs, and nuclear technology applications [1–3]. Thulium (Tm) is a rare-earth element with a single stable isotope, ^{169}Tm. Due to its high neutron sensitivity, ^{169}Tm plays a vital role in the nuclear industry [4–6]. However, data on the neutron total cross section of ^{169}Tm in the keV region in the Experimental Nuclear Reaction Data library are limited. As shown in Fig. 1, only three datasets have been reported in this range, including single-point data reported by Vertebnyy [7] and Dilg [8] and data with high uncertainty from Tellier [9]. A significant gap exists in the data between 5 keV and 2.3 MeV. The bottom panel shows clear discrepancies among the evaluated nuclear data libraries ENDF/B-VIII.1 [10], JENDL-5 [11], JEFF-3.3 [12], BROND-3.1 [13], and TENDL-2023 [14] in the keV energy range. To accurately measure the neutron total cross section of ^{169}Tm in the keV energy range, a measurement was performed at the back-streaming white neutron beam line (Back-n) of the China Spallation Neutron Source (CSNS) using a wing-shaped lithium glass detector. The detector was used to measure the in-beam γ-ray with a saturated resonance absorption technique. The neutron total cross section of ^{169}Tm was determined in the energy range of 1 keV to 110 keV. Theoretical calculations for the energy region were subsequently performed using optimized optical model parameters in TALYS-2.0 for comparison and validation.

II. EXPERIMENTAL METHOD

The measurement of the neutron total cross section was performed using the transmission method combined with the time-of-flight (TOF) technique. The neutron transmission $T_{exp}(E_i)$ at a neutron energy E_i is obtained as

Received 30 October 2025; Accepted 30 December 2025; Accepted manuscript online 31 December 2025

* This work was supported by the National Natural Science Foundation of China (12475308), National Key Research Program of China (2023YFA1606603) and the Continuous-Support Basic Scientific Research Project (BJ010261223282)

† E-mail: renjie@ciae.ac.cn

‡ E-mail: ruanxc@ciae.ac.cn

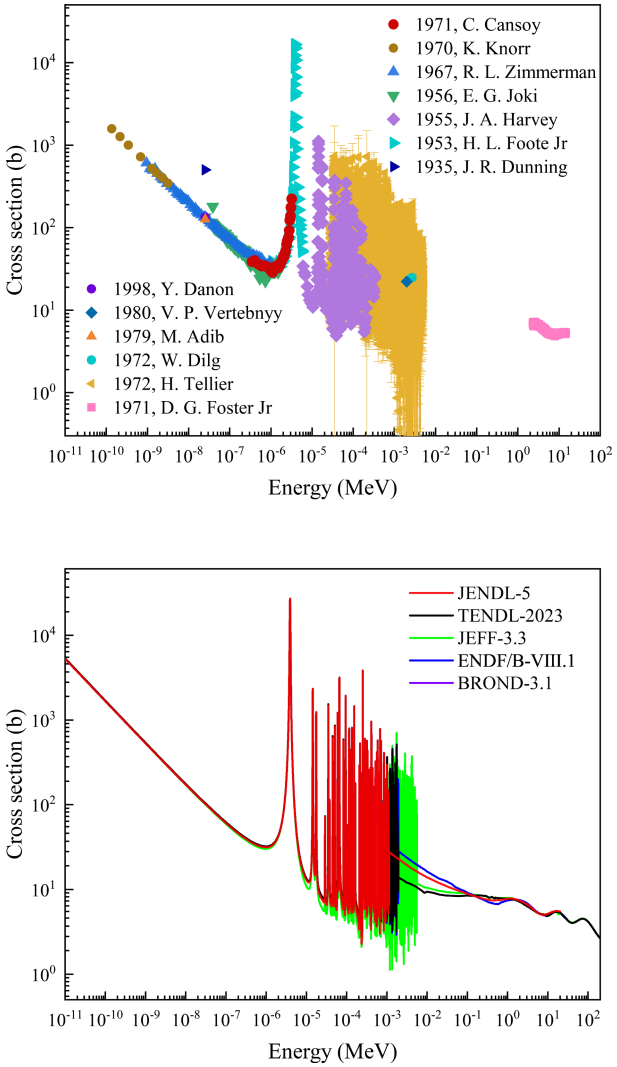

Fig. 1. (color online) Experimental cross section of ^{169}Tm from the EXFOR database (top panel) and evaluated cross section from ENDF/B-VIII.1, JENDL-5, JEFF-3.3, TENDL-2023, and BROND-3.1 libraries (bottom panel).

the ratio of the background-subtracted neutron counts with and without the sample. It is given by

$$T_{\rm exp}(E_i) = \frac{C_{\rm in}(E_i) - B_{\rm in}(E_i)}{C_{\rm out}(E_i) - B_{\rm out}(E_i)}, \tag{1}$$

where $C_{\rm in}(E_i)$ and $B_{\rm in}(E_i)$ are the neutron counts and background counts, respectively, under the sample-in conditions. $C_{\rm out}(E_i)$ and $B_{\rm out}(E_i)$ are the neutron counts and background counts, respectively, under the sample-out conditions. From the measured transmission $T_{\rm exp}(E_i)$, the total cross section $\sigma_{\rm t}(E_i)$ can be determined by

$$\sigma_{\rm t}(E_i) = -\frac{1}{n}\ln T_{\rm exp}(E_i), \tag{2}$$

where n is the areal density of the sample. The neutron energy was measured with the TOF method. The non-relativistic energy equation can be expressed as

$$E_i = \frac{m_n L^2}{2(t-t_0)^2} = \frac{k^2 L^2}{(t-t_0)^2}, \tag{3}$$

where E_i is the neutron energy, m_n is the neutron mass, t_0 is the time of neutron production, t is the arrival time of the neutron. $k \approx 72.2996\left[\sqrt{\rm eV}\cdot\mu{\rm s/m}\right]$.

III. EXPERIMENTAL METHOD

A. The Back-n beam

At the CSNS Back-n facility, neutrons are produced by a 1.6 GeV/c proton beam striking a tungsten target. The beam was operated in a double-bunch mode at 25 Hz, with each pulse containing two 42-ns-wide bunches separated by 410 ns. The experimental layout is shown in Fig. 2. The Back-n area includes two experimental stations designated as Experimental Station 1 (ES#1) and Experimental Station 2 (ES#2). Three collimators located at 24 m, 50 m and 70 m from the spallation target are utilized to adjust the shape of neutron beam spot. The first collimator is a beam shutter and equipped with filters. For measurements of the neutron total cross section, the inner diameters of the three collimators were 3 mm, 15 mm, and 40 mm. The detector surface was approximately 21 m from the sample center, while the sample center was about 56 m from the spallation target center. This configuration can reduce the background from scattered neutrons.

B. Neutron detector

At present, the measurements of the neutron total cross section carried out at CSNS Back-n [15, 16] are primarily based on the neutron total cross section spectrometer (NTOX) [17–21]. In this study, a glass scintillator detector with smooth detection efficiency was employed as shown in Fig. 3. Coincidence measurements between two PMTs can significantly reduce dark-noise signals and improve the signal-to-background ratio. The 0.1-mm-thick titanium (Ti) foils were used to seal the detector along the beam direction to reduce the background from scattered neutrons.

The neutron detection principle of glass scintillators is based on the exothermic nuclear reaction ^{6}Li$(n,\alpha)^3$H. Although both ^{6}Li and ^{7}Li respond to γ-ray, only ^{6}Li exhibits its obvious sensitivity to neutrons. The ^{7}Li-GS detector was employed to quantify the in-beam γ-ray background, which was then subtracted from the ^{6}Li-GS detector to obtain neutron-induced events accurately. Each photomultiplier tube (PMT) was independently powered by a high-voltage (HV) supply, and the output signal of the

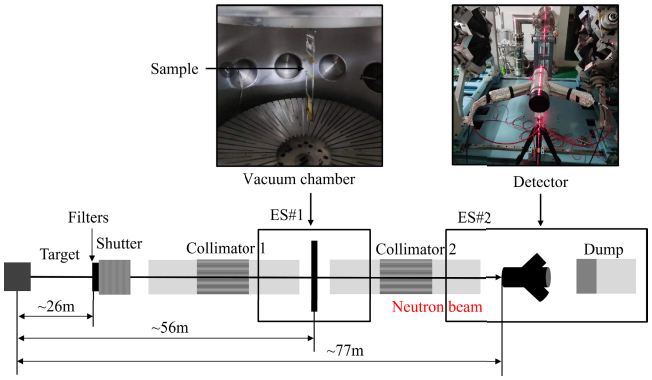

Fig. 2. (color online) Schematic diagram of neutron total cross section measurement facility. The sample was set at a vacuum chamber equipped with a remotely controlled sample-changing system. A wing-shaped lithium glass detector was employed at ES#2.

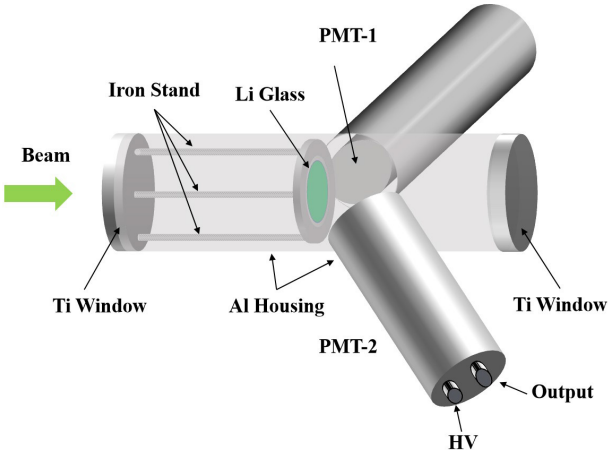

Fig. 3. (color online) Structure of the detector. It consists of three coupled aluminum tubes. The central tube is aligned with the beam, where a ^{6}Li-glass scintillator (^{6}Li-GS) and a ^{7}Li-glass scintillator (^{7}Li-GS) can be installed interchangeably. The PMTs are housed in the side tubes set at 60° to the central axis, reducing the blinding effect of the γ-flash.

PMT and the pulsed proton beam signal were fed to a CAEN DT5730B unit for digitization.

C. Sample and filters

The sample shown in Fig. 4 was placed in a vacuum chamber at ES#1. The filters were located near the neutron beam window. To subtract the background accurately, the measurement was performed with the black resonance filter method to determine the background. Therefore, the filters should be selected from materials with large neutron absorption cross sections and narrow resonance peaks such as cadmium (Cd), tantalum (Ta), cobalt (Co), and silver (Ag). In this experiment, the filters selected were 1 mm ^{181}Ta and 1 mm ^{59}Co. Additionally, the 1 mm ^{nat}Cd filter was employed to block thermal neutrons effectively and prevent overlap between consecutive

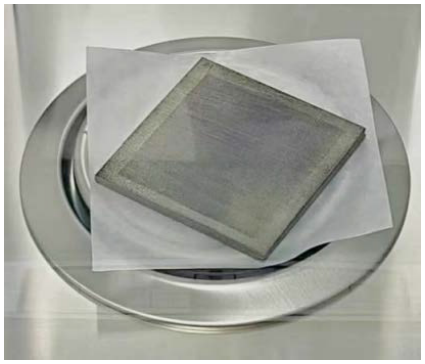

Fig. 4. (color online) The sample is square with a size of 60.37 mm × 4.46 mm.

neutron pulses to enhance the accuracy of the measurement. Detailed information on the sample and filters is provided in Table 1.

IV. DATA ANALYSIS

Events with signals detected by both PMTs within a coincident-time window were identified as valid coincidences. The waveforms of all triggered events were recorded, including those induced by γ-rays and neutrons. To accurately assess the experimental background, data were analyzed for both the sample-in and sample-out conditions using two types of scintillators (^{6}Li-GS and ^{7}Li-GS, respectively). The total counts measured by the ^{6}Li-GS detector included contributions from neutron events, activation background, and in-beam γ-rays. The measured transmission was then expressed as

$$T_{\rm exp} = \frac{C_{\rm in}\times f_1 - B_{0\rm in}\times f_1 - k_{\rm in}\times B_{\gamma\rm in}\times f_2}{C_{\rm out}\times f_3 - B_{0\rm out}\times f_3 - k_{\rm out}\times B_{\gamma\rm out}\times f_4}, \quad (4)$$

where $C_{\rm in}$ and $B_{0\rm in}$ are the total counts and flat background counts, respectively, measured by the ^{6}Li-GS detector under the sample-in conditions, whereas $C_{\rm out}$ and $B_{0\rm out}$ correspond to those measured by the ^{6}Li-GS detector under the sample-out conditions. $B_{\gamma\rm in}$ and $B_{\gamma\rm out}$ are the in-beam γ-rays obtained using the ^{7}Li-GS detector for the sample-in and sample-out states, respectively. f_1, f_2, f_3, and f_4 represent the product of the factors accounting for the dead-time correction and the proton-count normalization for each measurement. Additionally, $k_{\rm in}$ and $k_{\rm out}$ are factors determined from the TOF spectra measured by the ^{7}Li-GS detector with the saturated resonance absorption technique.

A. Determination of neutron energy and flight length

Precise determination of neutron energy relies on accurate calibration of the neutron TOF and flight length. The raw flight time ($\rm TOF_{raw}$) was obtained from the difference between the neutron arrival time and the initial

Table 1. Sample and filter parameters, including material, shape, length, diameter, thickness and purity are listed.

Material	Shape	Length/Diameter /mm	Thickness /mm	Purity (%)
^{169}Tm	Square	60.37 ± 0.11	4.46 ± 0.05	99.95
^{181}Ta	Square	100.00 ± 0.10	1.00 ± 0.01	99.90
^{59}Co	Square	100.00 ± 0.10	1.00 ± 0.01	99.90
^{nat}Cd	Circular	80.00 ± 0.10	1.00 ± 0.01	99.95

time. Given that the initial time recorded by the facility corresponded to the proton beam striking the target rather than the actual neutron emission, the effective neutron time of flight (TOF_n) was obtained by subtracting the γ-flash TOF from $\mathrm{TOF}_{\mathrm{raw}}$. The TOF_n is expressed as

$$\mathrm{TOF}_n = \mathrm{TOF}_{\mathrm{raw}} - \left(T_\gamma - \frac{L}{c}\right), \tag{5}$$

where T_γ is the arrival time of γ-flash, determined by fitting the γ-flash peak in the $\mathrm{TOF}_{\mathrm{raw}}$ spectrum. c represents the speed of light. L is the effective flight length that incorporates neutron moderation and transport in the production target as well as propagation along the beamline. The flight length can be calibrated using the known energies and corresponding TOF of resonance peaks from filters and sample. In this study, the resonance peaks were selected for calibration: ^{181}Ta (13.91 eV, 23.95 eV, 39.15 eV, 63.16 eV, 82.98 eV, 99.36 eV, 166.49 eV, 194.90 eV, 225.21 eV), ^{169}Tm (65.76 eV, 250.81 eV), and ^{59}Co (2861.50 eV, 4328.27 eV). The flight length was determined by fitting the functional relation between neutron energy and $\mathrm{TOF}_{\mathrm{raw}}$ according to Eq. (3). According to the fitting of neutron energy and flight time in Fig. 5, L was determined to be 77.10 ± 0.05 m.

B. Correction and normalization

During measurements, if the system were unable to register a new pulse before completing the processing of the previous one, subsequent pulses could be lost. This dead-time effect depends on the characteristics of the detector and the configuration of the acquisition system. In this study, the data acquisition system was able to record nearly all triggered signals. However, a nonparalyzable dead-time model was employed to account for pile-up effects accurately. An effective dead-time of $\tau = 380$ ns was used, during which multiple pulses were treated as a single event. The correction method described by Knoll [22] can be applied, and the dead-time correction factor f_{dt} is given as

$$f_{\mathrm{dt}} = \frac{1}{1 - \tau N_i}, \tag{6}$$

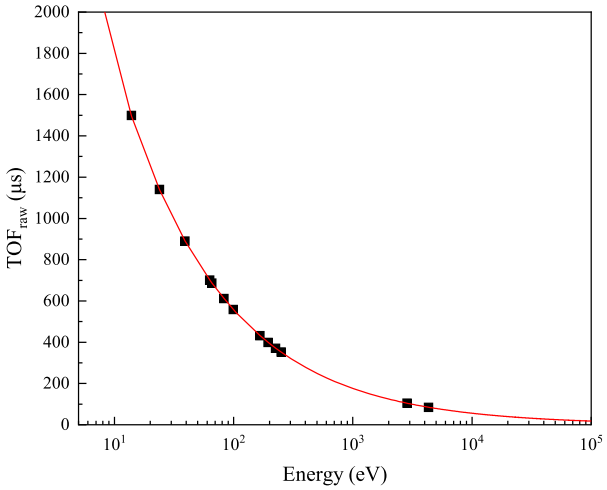

Fig. 5. (color online) Neutron flight length fit: experimental data (black points) and the fitted result (red curve).

where N_i is the counts normalized to the proton pulse and bin width. The variation of f_{dt} as a function of TOF is shown in Fig. 6. Above 16,700 ns (corresponding to neutron energy below 110 keV), the correction factors for the ^{6}Li-GS and ^{7}Li-GS detectors decreased with increasing TOF. Within this range, count losses remained below 10%, which indicates that the data were reliable and suitable for further analysis. To correct for beam fluctuations and differences in measurement duration, each spectrum was normalized using the reciprocal of the corresponding proton count before background subtraction.

C. Background analysis

The background in neutron total cross section measurements includes both time-independent and time-dependent components. The time-independent background arises from environmental and sample radioactivity and remains constant over time as a flat background. The time-dependent background includes sample-dependent and sample-independent parts, which primarily originate from in-beam γ-rays with energies ranging from keV to several tens of MeV [23]. The sample-independent background was measured using a ^{7}Li-GS detector with the saturated resonance technique. Given the large neutron cross section of ^{169}Tm at 3.90 eV, it is assumed that all neutrons at this energy are absorbed [24] and thus form an obvious absorption valley in the TOF_n spectra. This feature was used to determine the level of in-beam γ-ray background. The total background of the ^{6}Li-GS detector under the sample-in conditions, B_{Li6in} can be expressed as

$$B_{\mathrm{Li6in}} = B_{0\mathrm{Li6in}} + [C_{\mathrm{Li7in}} - B_{0\mathrm{Li7in}}] \times k_{\mathrm{in}}, \tag{7}$$

where $B_{0\mathrm{Li6in}}$ is the flat background of the ^{6}Li-GS detector, C_{Li7in} is the measured counts of the ^{7}Li-GS detector,

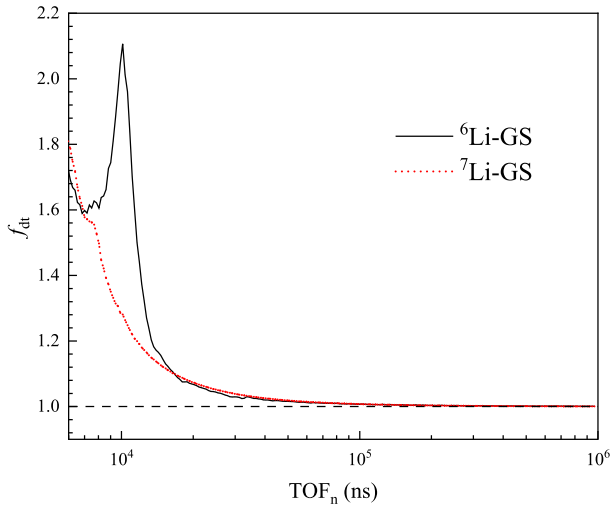

Fig. 6. (color online) Variation of the dead-time correction factor with flight time. The black solid line represents the values for ^{6}Li–GS detector without the filters or sample, while the red short-dashed line represents those for ^{7}Li–GS detector.

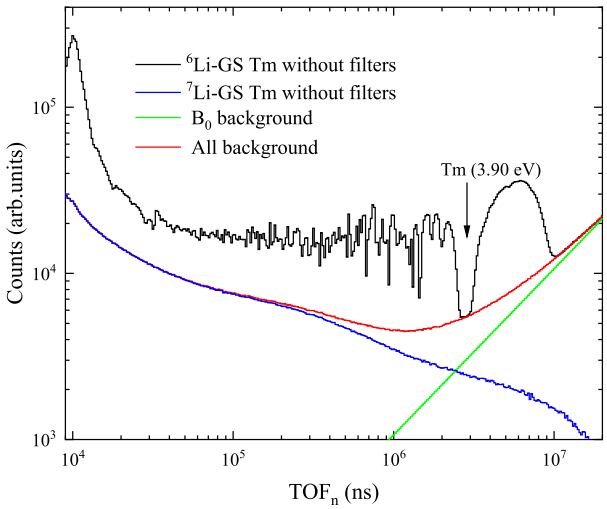

Fig. 7. (color online) Background with the sample using the ^{6}Li-GS and ^{7}Li-GS detectors. The green curve represents the flat background, the blue curve represents the in-beam γ-ray background, and the red curve shows the total background contributing to the TOF spectrum measured by the ^{6}Li-GS detector (black curve).

and $B_{0\mathrm{Li7in}}$ is the flat background of the ^{7}Li-GS detector. The background measured by the ^{6}Li-GS detector for ^{169}Tm without filters is shown in Fig. 7. k_{in} is determined to be 0.43 according to the valley at 3.90 eV. The in-beam γ-rays spanned the entire energy range and became more dominant at higher energies, while the flat background mainly affected the region above 10^6 ns (below 30 eV).

Under the sample-out conditions, the absence of the sample absorption peak made it impossible to determine the in-beam γ-ray normalization factor directly. Instead, it was obtained using the ^{7}Li-GS detector combined with the black resonance filter technique. Filters with strong cross section at neutron resonance absorption peaks were employed to fully absorb neutrons at specific energies [25] to create black resonance valleys in the spectra. As shown in Fig. 8, distinct valleys were observed at the resonance peaks of ^{59}Co (132 eV, 5.036 keV) and ^{181}Ta (4.28 eV) where most incident neutrons were absorbed, and the remaining part corresponds to the background. The background of the ^{6}Li-GS detector without filters can be determined by

$$B_{\mathrm{Li6out}} = B_{0\mathrm{Li6out}} + [C_{\mathrm{Li7out}} - B_{0\mathrm{Li7out}}] \times k_{\mathrm{f}}/k_{\mathrm{a}}, \qquad (8)$$

where B_{Li6out} is the total background of the ^{6}Li-GS detector without sample or filters. $B_{0\mathrm{Li6out}}$ is the flat background of the ^{6}Li-GS detector. C_{Li7out} is the measured counts of the ^{7}Li-GS detector, and $B_{0\mathrm{Li7out}}$ represents the flat background of the ^{7}Li-GS detector. Similarly, k_{f} is the normalization factor for in-beam γ-rays, which was determined as 0.42 from Eq. (7). In Fig. 8, the top panel shows the background composition of the ^{6}Li-GS detector with filters. The background curve passed through the obvious resonance peaks of ^{181}Ta (4.28 eV) and ^{59}Co (132 eV). k_a is the attenuation factor of the in-beam γ-rays due to the filters. To determine the attenuation factor k_a, the in-beam γ-ray spectra with and without the filters were simulated using the Geant4 toolkit (version 10.7.4) [26–28]. As shown in Fig. 9, the output shows the simulated γ-ray energy spectra measured by the ^{7}Li-GS detector. Given that the energy distribution of in-beam γ-rays remained invariant over different neutron flight time intervals [23], k_{a} was determined to be 0.91 [29]. The deviation between $k_{\mathrm{f}}/k_{\mathrm{a}}$ and k_{in} was within 5 %, which indicates the accuracy of the simulation and validates the reliability of the background estimation based on Eq. (8).

D. Self-shielding correction

After background subtraction, the average neutron transmission ($\bar{T}_{\mathrm{exp}}$) of ^{169}Tm can be determined using Eq. (4). However, the cross section directly calculated by $\bar{T}_{\mathrm{exp}}$ does not represent the real average total cross section ($\langle\sigma_t\rangle$). This study primarily focused on the URR in which individual resonance peaks overlap significantly, although the experimental resolution may not suffice to fully resolve them. According to the Hauser-Feshbach statistical model [30], the average total cross section $\langle\sigma_t\rangle$ can be statistically estimated as

$$\langle\sigma_t\rangle = \frac{1}{n}\ln\left(\mathrm{e}^{-n\sigma_t}\right) + \frac{1}{n}\ln\left[1 + \frac{n^2}{2}\mathrm{var}(\sigma_t) \pm \cdots\right]. \qquad (9)$$

As shown in Eq. (9), the first term corresponds to the quantity frequently misinterpreted as the experimental

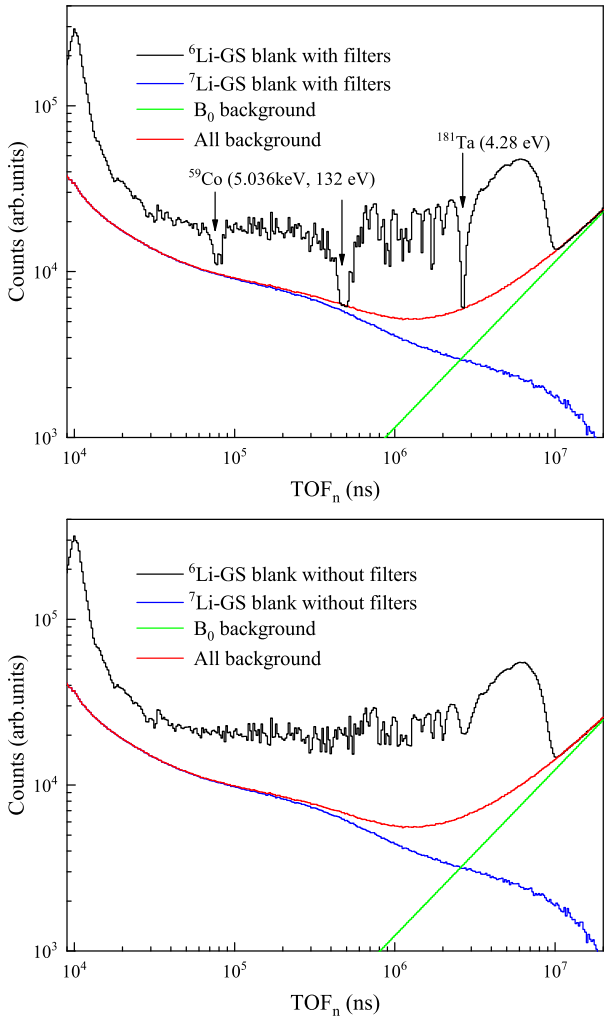

Fig. 8. (color online) Background composition without a sample measured by the ^{6}Li-GS and ^{7}Li-GS detectors. Top panel: background composition with filters. Bottom panel: background composition without filters.

total cross section in high-resolution measurements. The additional terms, which are frequently neglected in theoretical treatments, provide corrections involving the variance of the cross section and higher-order statistical moments to account for the contribution of unresolved resonances [31]. To incorporate the influence of resonant self-shielding in the URR, the self-shielding factor (F_T) is applied to the average transmission. It can be expressed as

$$F_T = \frac{\overline{T}_{exp}(E_i)}{e^{-n\langle\sigma_t\rangle}} \approx 1 + \frac{1}{2}n^2 \mathrm{var}(\sigma_t) \pm \cdots . \tag{10}$$

The self-shielding correction factor was calculated using the SESH code developed by Fröhner, which employs Monte Carlo sampling based on statistically generated resonance parameters and utilizes nuclear properties such as level spacing and strength functions [32]. As

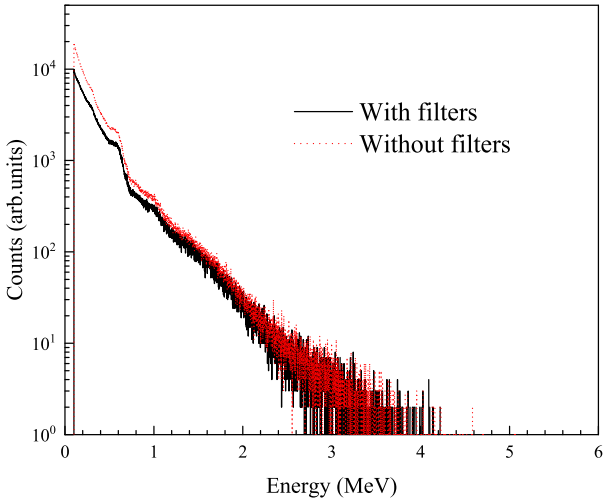

Fig. 9. (color online) Simulated spectra of the in-beam γ-ray energy for the ^{7}Li-GS detector. The solid line represents the values with filters, while the short-dashed line represents those without filters.

shown in Fig. 10, the factor decreases with increasing neutron energy and follows a double-exponential decay given by

$$y = A_1 \times e^{-x/a} + A_2 \times e^{-x/b} + A_3, \tag{11}$$

where $A_1 = 0.375 \pm 0.013$, $a = 0.823 \pm 0.033$, $A_2 = 0.069 \pm 0.003$, $b = 5.108 \pm 0.187$, and $A_3 = 1.001 \pm 0.001$. Fig. 11 shows a comparison between the transmission data with and without self-shielding correction. The corrected transmission was reduced to 0.87−0.99 of the original value. These results confirm that the application of the self-shielding correction significantly improved the accuracy and reliability of cross section measurements in the URR.

V. RESULT AND ANALYSIS

A. Neutron total cross section

The average total cross section $\langle\sigma_t\rangle$ defined in terms of the areal density of the sample and the transmission corrected for self-shielding is given as

$$\langle\sigma_t\rangle = -\frac{1}{n}\ln\left[\frac{T_{exp}(E_i)}{F_T}\right]. \tag{12}$$

As shown in Fig. 12, the neutron energy grid is intentionally sparse to obtain average total cross sections and optical model parameters. The measured total cross section appeared as a smooth curve and showed good agreement with both the evaluated nuclear data libraries and previous experimental results. In the energy range of

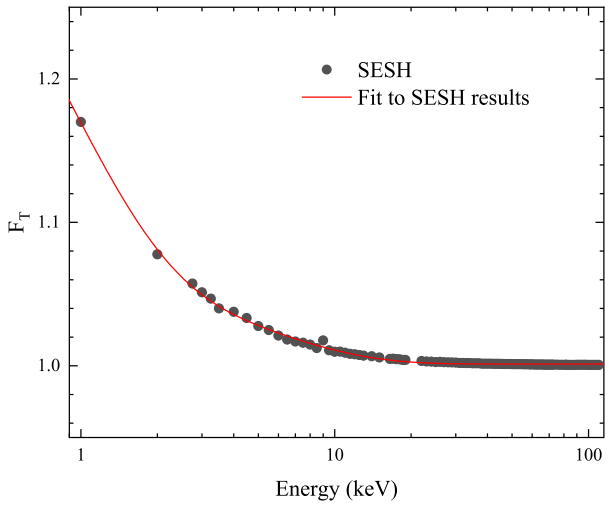

Fig. 10. (color online) Self-shielding correction factor. Black points represent the SESH simulation, and the red curve shows the fit. The factor remains below 1.01 for neutron energies above 10 keV.

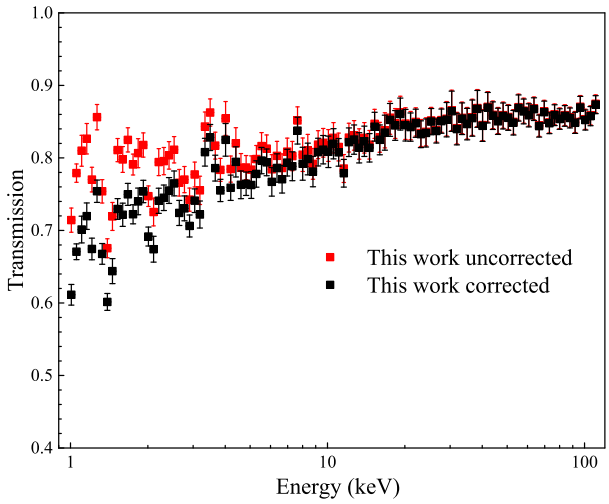

Fig. 11. (color online) Comparison of corrected (black) and uncorrected (red) transmissions from this study.

1−110 keV, it decreased from 33 b to 9 b with a generally declining trend. The results of this study can be used to fill the data gap in the 5−110 keV energy range. The measured value at 2.0 keV was 11% higher than that obtained by Vertebnyy [7], whereas at 2.7 keV, it was 13% lower than that reported by Dilg [8]. Among the evaluated libraries, the present results show the closest agreement with JENDL-5 evaluations. Minor deviations were observed from other evaluated libraries, with most points lying slightly above those of JEFF-3.3 and slightly below those of ENDF/B-VIII.1.

B. Uncertainty analysis

The analysis of uncertainty was primarily divided into two parts, including the energy uncertainty and the

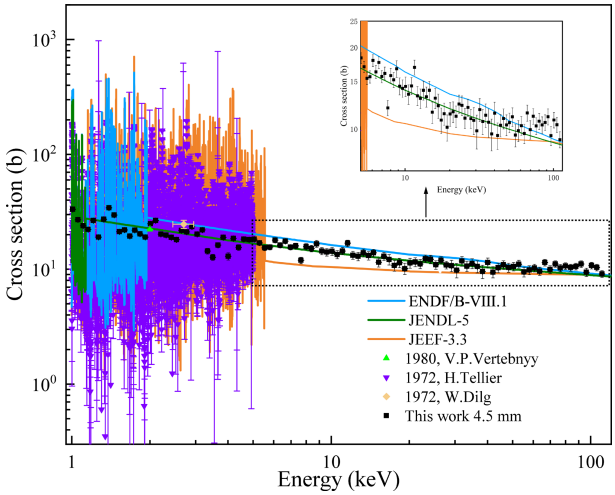

Fig. 12. (color online) Neutron total cross section measured in this study compared with ENDF/B-VIII.1 (blue), JENDL-5 (green), and JEFF-3.3 (orange) evaluations and EXFOR data.

cross section uncertainty. As shown in Eq. (3), the main uncertainties in the TOF neutron energy measurement stem from the flight time (ΔTOF) and flight length (ΔL). In the measurements, the proton beam pulse width was approximately 42 ns. According to the uncertainty propagation law, the energy uncertainty was calculated as

$$\frac{\Delta E}{E} = 2\times\sqrt{\left(\frac{\Delta L}{L}\right)^2+\left(\frac{\Delta \mathrm{TOF}}{\mathrm{TOF}}\right)^2}. \tag{13}$$

The relative uncertainty of the measured energy points was within 0.50%. The uncertainty in neutron transmission primarily arises from the statistical errors of the measured counts with and without the sample and can be expressed as

$$\left(\frac{\Delta T}{T}\right)^2 = \left(\frac{\Delta C_{\mathrm{in}}}{C_{\mathrm{in}}-B_{\mathrm{in}}}\right)^2+\left(\frac{\Delta B_{\mathrm{in}}}{C_{\mathrm{in}}-B_{\mathrm{in}}}\right)^2 + \left(\frac{\Delta C_{\mathrm{out}}}{C_{\mathrm{out}}-B_{\mathrm{out}}}\right)^2+\left(\frac{\Delta B_{\mathrm{out}}}{C_{\mathrm{out}}-B_{\mathrm{out}}}\right)^2. \tag{14}$$

All uncertainties were propagated based on single-σ counting statistics, where ΔT is the standard uncertainty of neutron transmission, and ΔC_{in}, ΔC_{out}, ΔB_{in}, and ΔB_{out} represent the statistical uncertainties of the ^{6}Li-GS detector and ^{7}Li-GS detector counts under the sample-in and sample-out conditions, respectively. The relative uncertainty of the transmission was below 2.0%. The relative uncertainty of the cross section is expressed as

$$\frac{\Delta\sigma_t}{\sigma_t} = -\frac{1}{\ln T}\cdot\left[\left(\frac{\Delta T}{T}\right)^2+(\ln T)^2\left(\frac{\Delta n}{n}\right)^2\right]^{\frac{1}{2}}. \tag{15}$$

where Δn is the standard uncertainty of the areal density

of the sample. The relative uncertainty of the areal density was approximately 0.19%, which was negligible compared to the uncertainty of the transmission. In the energy range of 1 keV to 3 keV, the relative uncertainty of the total cross section remained below 5%. In the energy range of 3 keV to 110 keV, most values were below 10%.

C. Optical model calculation

In this study, the excitation function of the ^{169}Tm (n,tot) was calculated using the TALYS-2.0 code. The global optical model parameters (OMPs) proposed by Koning and Delaroche were adopted with the default level density model of the code, which combined the constant temperature model and the Fermi gas model (ldmodel = 1). The photon strength function was described using the simplified modified Lorentzian model (SMLO, strength = 9) [14, 33]. Given the strong sensitivity of the neutron total cross section to OMPs, key parameters including the potential depths, radii, and diffusenesses of both the real and imaginary components were fine-tuned to enhance agreement with experimental data in the 1−110 keV energy range [33]. The adjusted parameters summarized in Table 2 were scaled by factors ranging from 0.9 to 1.15, while all other input settings were kept at default values. Notably, the radius (r_V) of the real volume potential was reduced by 10%, while its diffuseness (a_V) increased by 8%. Enhancements to the terms (*rwd*, *awd*, d_1, d_2) further strengthened neutron absorption in the energy region. Coupled-channels calculations were extended to include the $0^+ - 2^+ - 4^+ - 6^+ - 8^+$ states by setting maxrot = 4.

As shown in Fig. 13, both the default TALYS-2.0 results and the TENDL-2023 evaluations significantly underestimated the experimental data, whereas the calculations using optimized parameters reproduced the measured values more accurately. These improvements demonstrate better consistency with experimental results as well as a more realistic description of the neutron total cross section of ^{169}Tm. These optimized parameters serve as valuable reference for future calculations of the neutron total cross section of ^{169}Tm and further refinement of optical model parameters.

Table 2. Optical model parameters of unit, default value, adjusted value, and factor are listed.

Parameter	Unit	Default Value	Adjusted value	Factor
a_V	fm	0.653	0.705	1.08
r_V	fm	1.231	1.108	0.90
rvd	fm	1.255	1.443	1.15
rwd	fm	1.255	1.443	1.15
awd	fm	0.517	0.705	1.10
d_1	MeV	13.065	14.372	1.10
d_2	MeV^{-1}	0.0186	0.0205	1.10
maxrot	—	2	4	—

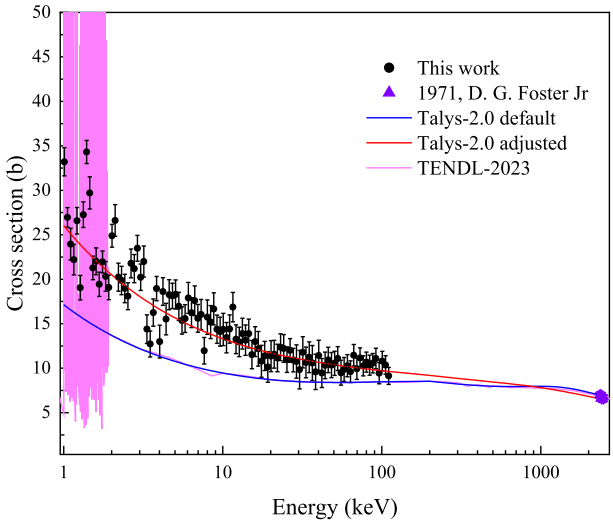

Fig. 13. (color online) Experimental data in the 1–110 keV range (black) compared with TALYS-2.0 calculations using default (blue) and adjusted (red) parameters and with evaluated data from TENDL-2023 (pink). When extended to 2.5 MeV, the adjusted parameters yield cross sections consistent with the results of Foster Jr. [34] in the 2.3–2.5 MeV range, with deviations mostly below 5%.

VI. CONCLUSION

The neutron total cross section of ^{169}Tm was measured in the energy range of 1−110 keV at the CSNS Back-n facility using a wing-shaped lithium glass detector. The in-beam γ-ray energy was quantitatively determined by combining the saturated resonance absorption technique with Monte Carlo simulations. Experimental neutron transmissions were obtained after dead-time correction, normalization, and background subtraction, with a relative uncertainty maintained within 2%. Self-shielding correction factors were calculated using the SESH code to derive the average total cross section. In the 1−110 keV energy range, most of corrected results showed good agreement with JENDL-5 evaluations, lying above the TENDL-2023 and JEFF-3.3 evaluations and below the ENDF/B-VIII.1 evaluations. The relative uncertainty of the total cross section was maintained below 5% in the 1−3 keV energy range and below 10% in the 3−110 keV energy range. The total cross section calculated using TALYS-2.0 with optimized optical model parameters agreed well with the experimental results and the data provided by Foster Jr. in the 2.3−2.5 MeV energy range, with most deviations within 5%.

Based on the present study, a systematic methodology for data acquisition and analysis has been established to measure the neutron total cross section with the wing-shaped lithium glass detector. However, there are

several aspects that require further improvement in the future. First, transmission experiments with samples of different thicknesses will be used to improve the accuracy of total cross section measurements. The thickness of the lithium glass scintillator used in this study was 4.0 mm, which resulted in an excessively high detection efficiency and a large measurement dead-time. The next step will involve optimizing the thickness of the lithium glass scintillator to reduce the dead-time and expand the measurable neutron energy range.

ACKNOWLEDGMENTS

The authors thank the staff members of the Back-n white neutron facility at the China Spallation Neutron Source (CSNS) for providing technical support and assistance in data collection and analysis.

References

[1] P. Schillebeeckx, B. Becker, Y. Danon *et al*., Nuclear Data Sheets **113**(12), 3054 (2012)
[2] R. Hannaske, Z. Elekes, R. Beyer *et al*., Eur. Phys. J. A **49**, 137 (2013)
[3] R. Beyer, A. R. Junghans, P. Schillebeeckx *et al*., Eur. Phys. J. A **54**, 81 (2018)
[4] K. B. Wang, L. T. Ma, C. Yang *et al*., Materials **16**(12), 4305 (2023)
[5] B. Jiang, J. L. Han, J. Ren *et al*., Chin. Phys. B **31**, 060101 (2022)
[6] I. M. Levinger and G. Shani, J. Nucl. Med. Radiat. Ther. **7**, 1000292 (2016)
[7] V. P. Vertebnyy, N. L. Gnidak, A. V. Grebnev *et al*., in All-union Conference on Neutron Physics (Kiev, Ukrainian SSR, 1980) pp. 249−253
[8] W. Dilg and H. K. Vonach, in Statistical Properties of Nuclei, edited by J. B. Garg (Springer, Boston, MA, 1972) pp. 327−334
[9] H. Tellier and M. Alix, *A study of the interaction of resonance neutrons with ^{169}Tm*, Symposium presentation (1972)
[10] D. A. Brown, M. B. Chadwick, R. Capote *et al*., Nucl. Data Sheets **148**, 1 (2018)
[11] O. Iwamoto, N. Iwamoto, S. Kunieda *et al*., J. Nucl. Sci. Technol. **60**, 1 (2023)
[12] A. J. Koning, O. Bersillon, R. A. Forrest *et al*., J. Korean Phys. Soc. **59**, 1057 (2011)
[13] A. I. Blokhin, E. V. Gai, A. V. Ignatyuk *et al*., Yad. Reak. Konst. **2**, 62 (2016)
[14] A. J. Koning, D. Rochman, J.-C. Sublet *et al*., Nucl. Data Sheets **155**, 1 (2019)
[15] Q. An, H. Bai, P. Cao *et al*., J. Instrum. **12**, P07022 (2017)
[16] H. S. Chen and X. L. Wang, Nat. Mater. **15**, 689 (2016)
[17] X. Y. Liu, Y. W. Yang, R. Liu *et al*., Nucl. Sci. Tech. **30**, 139 (2019)
[18] J. M. Xue, S. Feng, Y. H. Chen *et al*., Chin. Phys. C **47**(12), 124001 (2023)
[19] J. M. Xue, S. Feng, Y. H. Chen *et al*., Nucl. Sci. Tech. **35**, 18 (2024)
[20] J. B. Bai, J. Y. Tang, L. Q. Shi *et al*., Chin. Phys. C **48**(8), 084001 (2024)
[21] J. B. Bai, J. Y. Tang, L. Q. Shi *et al*., Phys. Lett. B **863**, 139355 (2025)
[22] G. F. Knoll, *Radiation Detection and Measurement*, 3rd ed. (Wiley, Hoboken, NJ, USA, 2000) p. 122
[23] J. Ren, X. C. Ruan, Y. H. Chen *et al*., Acta Phys. Sin. **69**(17), 172901 (2020)
[24] L. M. Richard, H. Joseph, and R. W. Ronald, Nucl. Instrum. Methods **164**(1), 213 (1979)
[25] D. B. Syme, Nucl. Instrum. Methods Phys. Res. **198**(2-3), 357 (1982)
[26] J. Allison, K. Amako, J. Apostolakis *et al*., Nucl. Instrum. Methods A **835**, 186 (2016)
[27] J. Allison, K. Amako, J. Apostolakis *et al*., IEEE Trans. Nucl. Sci. **53**(1), 270 (2006)
[28] S. Agostinelli, J. Allison, K. Amako *et al*., Nucl. Instrum. Methods A **506**, 250 (2003)
[29] J. C. Wang, J. Ren, W. Jiang *et al*., Nucl. Sci. Tech. **35**, 164 (2024)
[30] W. Hauser and H. Feshbach, Phys. Rev. **87**, 366 (1952)
[31] R. M. Bahran, *New high energy resolution neutron transmission detector at the Gaerttner LINAC Center and isotopic molybdenum total cross section measurements in the keV-region*, Ph.D. Thesis, (New York: Rensselaer Polytechnic Institute, 2013)
[32] F. Fröhner, *SESH – A FORTRAN-IV code for calculating self-shielding and multiple scattering effects for neutron cross-section data interpretation in the unresolved resonance region*, Tech. Rep. GA-8380 (La Jolla, CA: Gulf General Atomic Inc., 1968)
[33] A. J. Koning, S. Hilaire, and S. Goriely, Eur. Phys. J. A **59**, 131 (2023)
[34] D. G. Foster Jr. and D. W. Glasgow, Phys. Rev. C **3**, 576 (1971)